Nano Energy 28 (2016) 447–454

Contents lists available at ScienceDirect

Nano Energy

journal homepage: www.elsevier.com/locate/nanoen

Flexible and ion-conducting membrane electrolytes for solid-state lithium batteries: Dispersion of garnet nanoparticles in insulating polyethylene oxide

Jingxian Zhang [a,b], Ning Zhao [b], Miao Zhang [a], Yiqiu Li [b], Paul K. Chu [c], Xiangxin Guo [b,*], Zengfeng Di [a,*], Xi Wang [a], Hong Li [d]

[a] State Key Laboratory of Functional Materials for Informatics, Shanghai Institute of Microsystem and Information Technology (SIMIT), Chinese Academy of Sciences (CAS), 865 Changning Road, Shanghai 200050, People's Republic of China
[b] State Key Laboratory of High Performance Ceramics and Superfine Microstructure, Shanghai Institute of Ceramics, Chinese Academy of Sciences (SICCAS), 1295 Dingxi Road, Shanghai 200050, People' s Republic of China
[c] Department of Physics and Materials Science, City University of Hong Kong, 83 Tat Chee Avenue, Kowloon, Hong Kong, People's Republic of China
[d] Institute of Physics, Chinese Academy of Sciences (CAS), 8 Zhongguancun South 3rd Street, Beijing 100190, People' s Republic of China

ARTICLE INFO

Article history:
Received 17 July 2016
Received in revised form
1 September 2016
Accepted 1 September 2016
Available online 2 September 2016

Keywords:
Flexible solid-state electrolyte
Ionic conductivity
Percolation behavior
Solid-state lithium battery

ABSTRACT

Solid-state electrolytes with high ionic conductivity, large electrochemical window, good mechanical properties, and easy processability are needed for high-energy solid-state lithium batteries. In this work, composite membranes consisting of lithium garnet (i.e. $Li_{6.4}La_3Zr_{1.4}Ta_{0.6}O_{12}$, LLZTO) particles and Li-salt-free polyethylene oxides (PEOs) are produced as solid-state electrolytes. Li-ion-conducting particles in nano-scale are crucial for the enhancement of conductivity and the membranes containing ~40 nm LLZTO particles exhibit conductivities nearly two orders of magnitude larger than those with the micro-scale ones, which is attributed to the difference in specific surface area related to the percolation effect. Compared to the conventional PEO doped with lithium salt, the insulating PEO in PEO:LLZTO membrane electrolyte is conducive to the suppression of lithium dendrite growth owing to prohibition of current flow. With PEO:LLZTO membrane electrolytes in conductivity of 2.1×10^{-4} S cm^{-1} at 30 °C and 5.6×10^{-4} S cm^{-1} at 60 °C, the solid-state $LiFePO_4$/PEO:LLZTO/Li and $LiFe_{0.15}Mn_{0.85}PO_4$/PEO:LLZTO/Li cells deliver energy densities of 345 Wh kg^{-1} (662 Wh L^{-1}) and 405 Wh kg^{-1} (700 Wh L^{-1}) (without the package weight or volume) with good rate capability and cycling performance. This study suggests that the conjunction of nano-scale Li-ion-conducting particles and an insulating polymer provides a promising solution to produce powerful solid-state electrolytes for high-performance solid-state lithium batteries.

1. Introduction

Solid-state lithium batteries (SSLBs) offer higher energy density, longer cycle life, and better safety than traditional Li-ion batteries [1–4]. The ideal SSLB uses metallic lithium as the anode, a highly Li-ion-conducting solid-state electrolyte (SSE) as the separator, and a composite cathode. Since there is no liquid component, the SSLB units can be densely packed thereby enhancing the volumetric energy density. Moreover, the stability of SSE (e.g. garnet-type electrolytes) allows the use of a metallic lithium anode as well as high-voltage cathode consequently increasing the gravimetric energy density.

However, the development of high-performance SSLB faces challenges and the priority is the ionic conductivity of SSE. With respect to the latter issue, much progress has been made in recent years [5–9]. Sulfide-based electrolytes show ionic conductivity as high as 10^{-1} S cm^{-1} [10–12] which is comparable to that of a liquid electrolyte. Oxide-based electrolytes such as perovskites, LISICONs, and garnets have ionic conductivities of ~10^{-2} S cm^{-1} [13], ~10^{-4} S cm^{-1} [14,15], and ~10^{-3} S cm^{-1} [16] at 30 °C, respectively. Although polymer-based electrolytes such as polyethylene oxide (PEO)-based ones show relatively small conductivity of ~10^{-5} S cm^{-1} at room temperature [17,18], the microporous complex polymer electrolytes based on polyvinylidene fluoride (PVDF)/PEO star polymer can deliver conductivity as high as ~10^{-3} S cm^{-1} [19]. In general, the SSE with ionic conductivity over 10^{-4} S cm^{-1} at room temperature is essential for the SSLB. In addition, the reliable stability and the interfacial resistance are also vital for SSLB with high performance. For instance, sulfides are too reactive in air thus complicating large-scale production [20],

* Corresponding authors.

http://dx.doi.org/10.1016/j.nanoen.2016.09.002
2211-2855/

perovskites and LISICONs are unstable against metallic lithium consequently limiting the energy density [21,22]. Furthermore, polymers are generally electrochemically unstable at a high potential thus hindering combination with high-voltage cathodes. In this respect, garnets are stable against metallic lithium and have a large electrochemical window. They have large resistance at grain boundaries and surface sensitivity to H_2O and CO_2 in air [23]. Unlike liquid electrolytes which can penetrate porous cathodes, adequate interfacial contact between the SSE and cathode is needed and there is concern about the construction of the ion-conducting network. Other issues include suppression of lithium dendrite growth and large-scale processability. The lithium dendrite growth has been shown to be serious in polymer-based electrolytes as well as in the Li/$Li_7La_3Zr_2O_{12}$ (LLZO)/Li cells with intermediate high-dense ceramic plates which are prone to short-circuit due to the inhomogeneous electric field at the Li/LLZO contact [24]. Flexible and sticky properties may also be required for SSEs when considering the expedient process to assemble SSLB.

To fulfill the aforementioned requirements, here, nano-scale LLZTO particles are dispersed in the insulating PEOs to form flexible 40 μm-thick composite membranes as the electrolytes. By taking advantage of the percolation behavior along the interface of highly Li-ion-conducting LLZTO particles/PEOs, the composite membranes provide high ionic conductivity more than 10^{-4} S cm^{-1} at 30 °C even though the PEOs are insulating. In addition, the insulating PEO allows distribution of spatial ionic current dominated by the LLZTO nanoparticles, which are beneficial to the improvement of electrochemical stability and the suppression of lithium dendrite growth. The composite membrane electrolytes are self-standing albeit with a thickness of only ~40 μm and can be easily attached to electrodes at 60 °C. With the integration of the composite membranes as the electrolytes, the SSLBs based on $LiFePO_4$/PEO:LLZTO/Li and $LiFe_{0.15}Mn_{0.85}PO_4$/PEO:LLZTO/Li exhibit good rate capability and cycle performance. Our study opens a new avenue for developing the potential Li-salt-free composite membrane electrolyte for high performance SSLB.

2. Experimental

2.1. Materials preparation

PEO (Mv = 10^6 g mol^{-1}, Aldrich) was dried at 60 °C overnight under vacuum prior to the sample preparation. LiTFSI (99.95%, Sigma-Aldrich), $LiClO_4$ (99.99%, Sigma-Aldrich), anhydrous acetonitrile (ACN), succinonitrile (SCN), PVDF (Aladdin), super-P conductive additives (SP, Timcal), $LiFePO_4$ (LFP) and $LiFe_{0.15}Mn_{0.85}PO_4$ (LFMP) were used as received. All the procedures sensitive to moisture or oxygen were carried out in an Ar-filled glovebox (M-Braun, Germany) with H_2O and O_2 contents below 0.1 ppm. The sizes of LLZTO particles were controlled by the ball milling processes. For instance, the starting ~10 μm LLZTO particles were reduced to ~3 μm by planetary ball-milling. With high-energy ball-milling (0.1 mm diameter zirconia balls) with the protection of Ar atmosphere, the sizes of LLZTO particles could be further shrunk to ~400 nm, ~200 nm or ~40 nm. The corresponding size distributions and SEM images are displayed in Fig. S1. The PEO:LLZTO and PEO:LiTFSI:LLZTO membranes were prepared by mixing pre-weighed amounts of PEO, LLZTO, and LiTFSI in ACN and the typical thickness of the membrane was ~40 μm. The amount of LiTFSI in PEO:LiTFSI and PEO:LiTFSI:LLZTO was determined by the molar ratio of –CH_2–CH_2O- (EO)/Li^+ (EO/Li^+ = 8).

2.2. Sample characterization

SEM (Hitachi S-3400N) equipped with an energy-dispersive X-ray spectroscopy detector (EDS) was employed to determine the microstructure as well as chemical composition of the samples. Optical microscopy (LEICA DM4000M) was performed to monitor lithium dendrite growth in the symmetric Li/SSE/Li cells. XRD was performed on the Bruker D2 Phaser with Cu K_α radiation (λ = 1.5406 Å) with 2θ in range of 10°–80° and step size of 0.02° s^{-1} to characterize the crystalline structure of ingredients and synthesized electrolytes. The particle size distribution was determined by a Zeta Plus (Brookhaven) laser particle size analyzer.

2.3. Electrochemical measurements and cells assembly

The conductivity of the SSE was determined by the NOVOCONTROL GmbH Concept 40 dielectric broadband spectrometer fitted with a Quatro temperature control system at a frequency range between 0.01 Hz and 4×10^7 Hz and temperature range from 30 °C to 100 °C. The block/SSE/block cell using stainless steel (SS) electrodes was used. The electronic conductivity was determined by potentiostatic polarization using the Li/SSE/Li cell at a voltage of 5 V on a battery test station (Arbin BT-2000). The pouch cells with approximately 0.1 Ah were used to evaluate the battery performance with PEO:LLZTO in which the lithium metals in thickness of ~50 μm pressed on Cu foils were used as the anodes, LFP or LFMP with PVDF:SCN:$LiClO_4$ binders with a weight ratio of LFP or LFMP:binder:SP = 8:1:1 were coated on Al foils to form the cathodes. The image of the typical pouch cell is depicted in Fig. S2. Linear sweep voltammetry (LSV, from 2.6 V to 6.0 V with the scan rate of 10 mV s^{-1}) and cyclic voltammetry (CV, from −0.5 V to 6.0 V with the scan rate of 10 mV s^{-1}) were conducted on the electrochemical workstation (Autolab, AUT30FRA2 ECICHEMIE) using Li/SSE/SS 2032 type coin cells with 8 mm diameter lithium metal electrodes and 12 mm diameter SSE films. The transference number was measured and calculated by alternating-current (AC) impedance and direct-current (DC) polarization (with a DC voltage of 10 mV) using the Li/SSE/Li cell. Lithium dendrite growth was monitored by the Arbin BT-2000 using symmetric Li/SSE/Li coin cells with 8 mm diameter lithium metal and 12 mm diameter SSE film. A current density of 3.0 mA cm^{-2} was applied to promote lithium deposition on the cathode. All the cells were prepared in an Ar-filled M-Braun glovebox.

3. Results and discussion

3.1. Characterization of the PEO:LLZTO membrane

The cubic LLZO is one of the most promising oxides for the SSE in the SSLBs because of the highly ionic conductivity with a unity transference number, chemical and electrochemical stability, and high mechanical strength with a shear modulus of 55 GPa [25,26]. Ta-doped LLZO (LLZTO) has been studied and it has a pure cubic garnet structure [27] as shown in Fig. S1. The ionic conductivity of LLZTO determined from a dense ceramic disk (diameter of 10 mm and thickness of 1 mm with the relative density of 99.6%) is 1.6×10^{-3} S cm^{-1} at 30 °C [28]. The pristine micro-scale LLZTO powders were ground by a dry ball mill (0.1 mm diameter zirconia balls) with protection of Ar atmosphere to produce nanoparticles of ~40 nm in size. As shown in Fig. 1a, the diameters of LLZTO particles in terms of D_{10}, D_{50} and D_{90} are 4.5 nm, 43 nm and 106 nm, respectively, which are calculated according to the reference [29]. Scanning electron microscopy (SEM) measurement presented in Fig. 1b further demonstrates that the particle size of

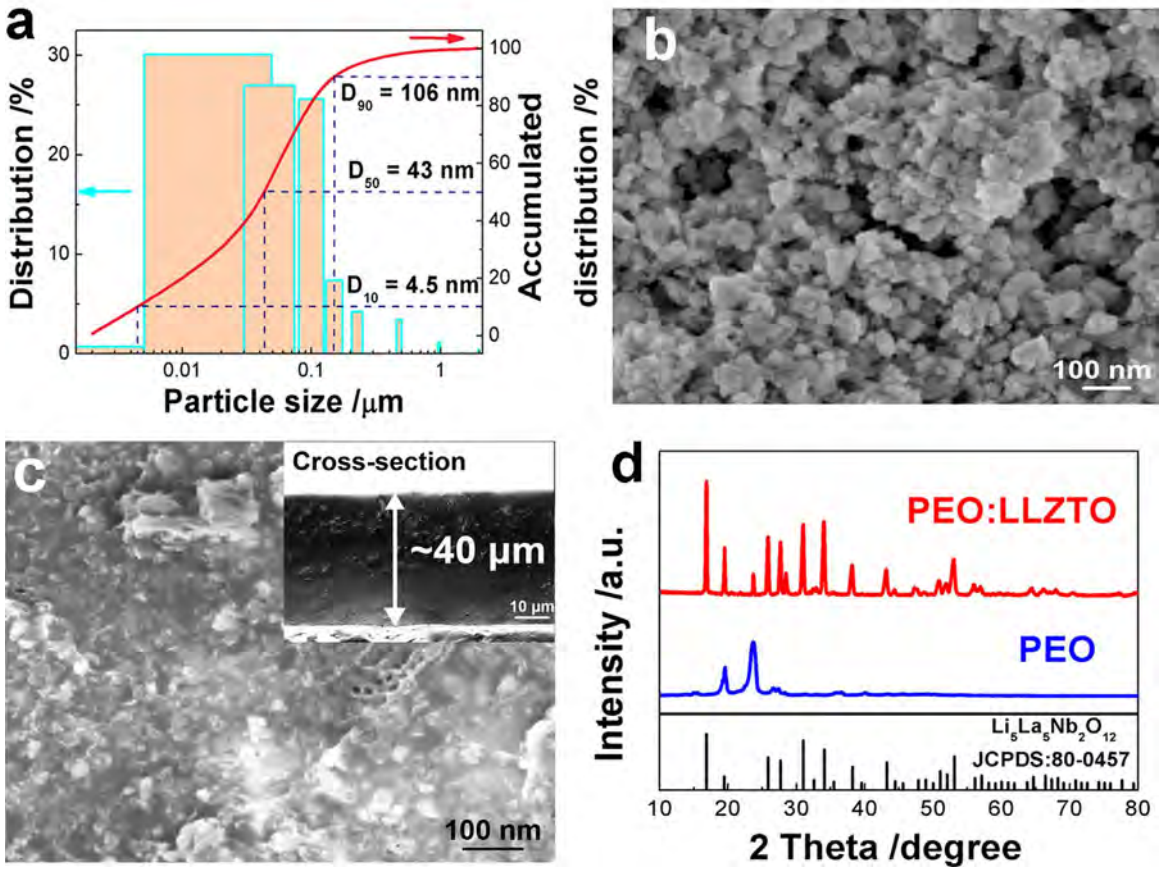

Fig. 1. Characterization of PEO:LLZTO membranes. (a) Size distribution of the LLZTO nanoparticles determined by a laser particle size analyzer. D_{10} of 4.5 nm, D_{50} of 43 nm, and D_{90} of 106 nm are calculated according to the reference [29]. (b) SEM of LLZTO nanoparticles. (c) Plane-view and cross-sectional (inset) SEM of 40 μm-thick PEO:LLZTO membrane. (d) XRD scan of the PEO:LLZTO membrane and PEO membrane. The JCPDS of $Li_5La_5Nb_2O_{12}$ indicates that LLZTO has a similar cubic phase.

LLZTO concentrates at ~40 nm. These nanoparticles are then dispersed in the insulating PEOs with a molecular weight of 10^6 g mol^{-1} in the glove box to form flexible 40 μm-thick composite membranes as the electrolytes (Fig. 1c). X-ray diffraction (XRD) scans obtained from typical PEO:LLZTO membrane show that the crystallinity of LLZTO has no change after mixing with PEO (Fig. 1d).

3.2. Ion transport properties of the PEO:LLZTO membranes

The conducting properties are investigated by AC impedance spectroscopy and the Nyquist plots are presented in Fig. 2a. According to Eq. 1,

$$\dot{o} = \frac{t}{RA} \tag{1}$$

where t is the thickness of each membrane, R is the resistance obtained by the simulation according to the equivalent circuit shown in Fig. S3, and A is the cross-section area, the conductivity is 2.1×10^{-4} S cm^{-1} at 30 °C and 5.6×10^{-4} S cm^{-1} at 60 °C. DC polarization is performed to evaluate the electron contribution (as shown in Fig. S4) and the electron conductivity is at least three orders of magnitude smaller than the overall conductivity, indicating dominance of ionic conduction.

The Arrhenius plots of the pure PEO membrane, LLZTO disk, and PEO:LLZTO membrane are displayed in Fig. 2b. According to Eq. 2,

$$\dot{o}T = A\exp\left(\frac{-E_a}{kT}\right) \tag{2}$$

where A is the pre-exponential factor, E_a is the activation energy, and T is the absolute temperature, the activation energy E_a of the PEO:LLZTO membrane is close to that of the LLZTO disk implying that the conduction of the composite membrane is dominated by the nanometer solid particles.

The conductivity as a function of the LLZTO (in size of D_{50}=43 nm) volumetric percentage is depicted in Fig. 2c. In the investigated temperature range, the maximum conductivity of PEO:LLZTO membrane is achieved at the LLZTO content of 12.7 vol% and this behavior has been observed from admixtures of oxides and polymer electrolytes [30–33]. It has been proposed that the dispersed oxide particles increase the carrier mobility on account of the enhanced segmental motion of the polymers as a result of the reduced degree of crystallinity [34,35]. It has also been proposed that the concentration increase in the mobile charge carriers plays a role in the conductivity enhancement, the so-called percolation behavior arising from the adsorption effect at the second-phase interface [32,35]. However, it was quite difficult to discern these two mechanisms previously because the polymers were frequently doped with a lithium salt [36–39]. In this work, apart from the interfacial region, the PEO is insulating due to the absence of lithium salt. Therefore, the possible change of PEO crystallinity due to the dispersed oxide particles will not affect the overall conductivity, which excludes the influence of the segmental motion. In contrast, the Li^+ in LLZTO can be absorbed by the polymer considering that the PEO may dilute the lithium salt by as much as 50 wt% [40]. This increases lithium vacancies which are mobile carriers on the LLZTO surface, thus increasing the overall conductivity in combination with the highly conducting LLZTO bulk. As a result, it is believed that the

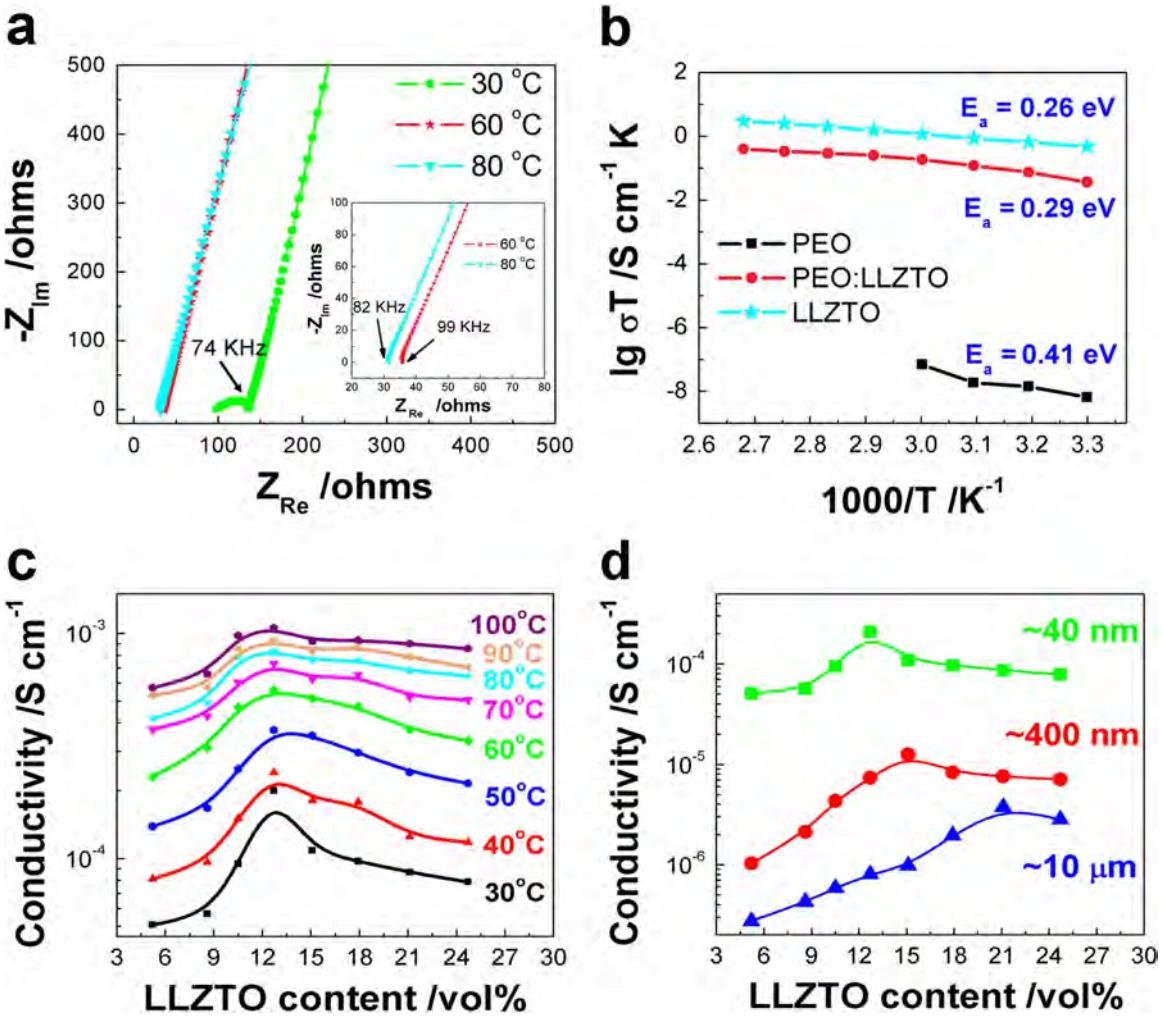

Fig. 2. Ion transport properties of the PEO:LLZTO membranes. (a) Impedance spectroscopy of the PEO:LLZTO membrane with a content of 12.7 vol% LLZTO in size of D_{50}=43 nm at different temperatures. The inset shows Nyquist plots in the region of high-frequency. (b) Arrhenius plots of the PEO, PEO:LLZTO membrane with 12.7 vol% LLZTO in size of D_{50}=43 nm, and LLZTO disks. (c) The conductivities of PEO:LLZTO membranes with different volume fractions of LLZTO in size of D_{50}=43 nm at different temperatures. (d) The conductivity as a function of LLZTO volume fraction for the LLZTO particles with different sizes.

percolation effect plays the important role in the conductivity enhancement. This is further supported by the particle-size effect on the conductivity, as shown in Fig. 2d. For the LLZTO particles with sizes of ~10 μm and ~400 nm, the corresponding conductivity maxima (3.8×10^{-6} S cm^{-1} and 1.3×10^{-5} S cm^{-1}, respectively) are obtained at the LLZTO content of 21.1 vol% and 15.1 vol%, which are larger than that of the ~40 nm particles (2.1×10^{-4} S cm^{-1} at 12.7 vol%), indicating that the percolation

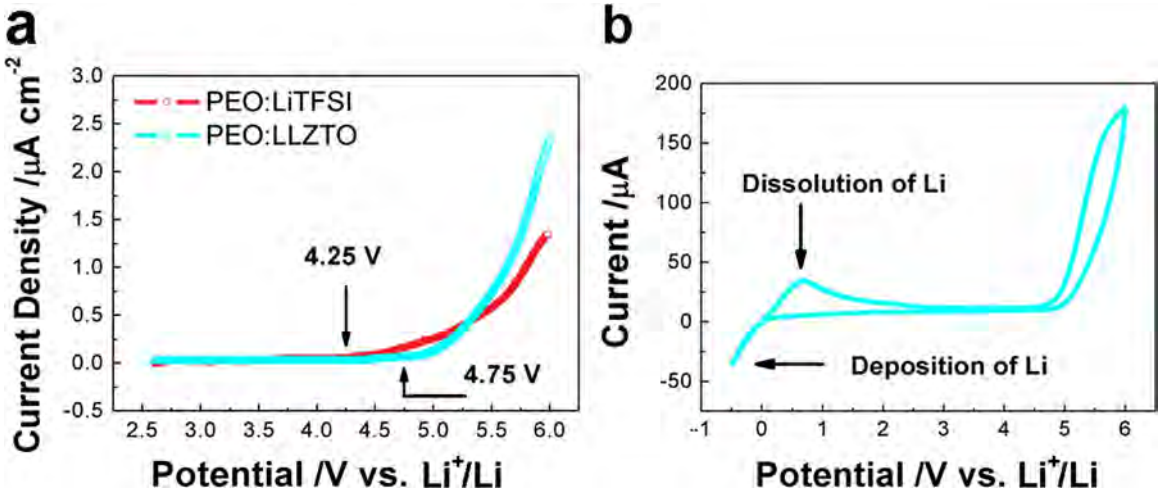

Fig. 3. Electrochemical window and stability of the PEO:LLZTO membrane. (a) LSV scans at a scanning rate of 10 mV s^{-1} for the PEO:LiTFSI and PEO:LLZTO membrane with 12.7 vol% LLZTO. (b) CV scans at a scanning rate of 10 mV s^{-1} of the PEO:LLZTO membrane with 12.7 vol% LLZTO.

threshold decreases with the decreasing particle size. Moreover, the membranes with the LLZTO particles in size of ~40 nm exhibit conductivities nearly two orders of magnitude larger than those with the micrometer-sized ones. The conductivity enhancement for LLZTO particles with smaller size is attributed to the highly conductive paths along the interfaces formed between the polymer matrix and ceramic grains [41], and small particles generally have a relatively large specific surface area, leading to the increase of coherent conductivity paths [42]. These results also imply that the nano-scale particles are more effective on improvement of conductivity compared to the micro-scale ones.

3.3. Critical factors of the membrane electrolyte

In addition to the ionic conductivity, there are other important issues when constructing the electrolytes for SSLBs, for example, (i) the stability against the metal lithium anodes and electrochemical window with respect to the cathodes, (ii) Li-ion transference number, and (iii) suppression of dendrite growth. Fig. 3a and b display the LSV (from 2.6 V to 6.0 V) and CV (from −0.5 V to 6.0 V) curves of the PEO:LLZTO membrane and the corresponding LSV curve of the PEO:LiTFSI membrane is shown for comparison. With regard to the PEO:LiTFSI, the oxidation process commences at 4.25 V. While the sweep can be extended to 4.75 V without an obvious current in the case of PEO:LLZTO (Fig. S5). The enhanced electrochemical stability can be attributed to the removal of impurities such as water from the interface by the inorganic ceramic fillers [43,44]. A similar phenomenon has been observed that the addition of LLZO to PEO increases the oxidation potential from 4.0 V to 5.0 V [45]. The transference number of Li^+ (i.e. T_{Li^+}) is calculated [40] as shown in the Supporting Information and Table S1. T_{Li^+} increases initially, approaches the maximum of 0.46 at 12.7 vol% and then decreases as the volume fraction of LLZTO further increases. This value is much greater than that of the PEO:LiTFSI (i.e. 0.22). It indicates that the LLZTO nanoparticles improve T_{Li^+} of the polymer electrolyte, and ion transport through the LLZTO nanoparticles and polymer/LLZTO boundaries are believed to account for such improvement.

Suppression of lithium dendrite growth is crucial to lithium metal anodes. The LLZTO ceramic disks have a large density and transference number of nearly unity. Serious lithium dendrite formation and penetration across disks are observed from the Li/LLZTO/Li cells during constant current density galvanostatic cycles at a current density of 0.5 mA cm^{-2}, which is attributed to the inhomogeneous contact between the LLZTO electrolytes and lithium anodes [46]. Here, the flexible and sticky polymers with large-surface-area LLZTO nanoparticles provide homogeneous contact between the electrolyte and the lithium anode. Fig. 4a and b show the constant current galvanostatic cycles of the Li/PEO:LLZTO/Li and the Li/PEO:LiTFSI:LLZTO/Li symmetrical cells, respectively. The applied constant current density is 3.0 mA cm^{-2}. The Li/PEO:LiTFSI:LLZTO/Li cell can only be operated for 25 h before short circuit occurs, but the Li/PEO:LLZTO/Li cell can be continuously operated for more than 700 h without short circuit. For Li/PEO:LLZTO/Li cell, the potential value is found to decrease as the operation duration extends due to the gradual activation of the PEO:LLZTO electrolyte. The cross-sectional optical microscopy images of the two cells indicate that the lithium metal in the Li/PEO:LLZTO/Li cell is flat without discernable dendrites, but many large dendrites are observed from the Li/PEO:LiTFSI:LLZTO/Li cell (Fig. 4c, d and Fig. S6). Formation of lithium dendrites in PEO:LiTFSI:LLZTO is responsible for the short circuit after a relatively

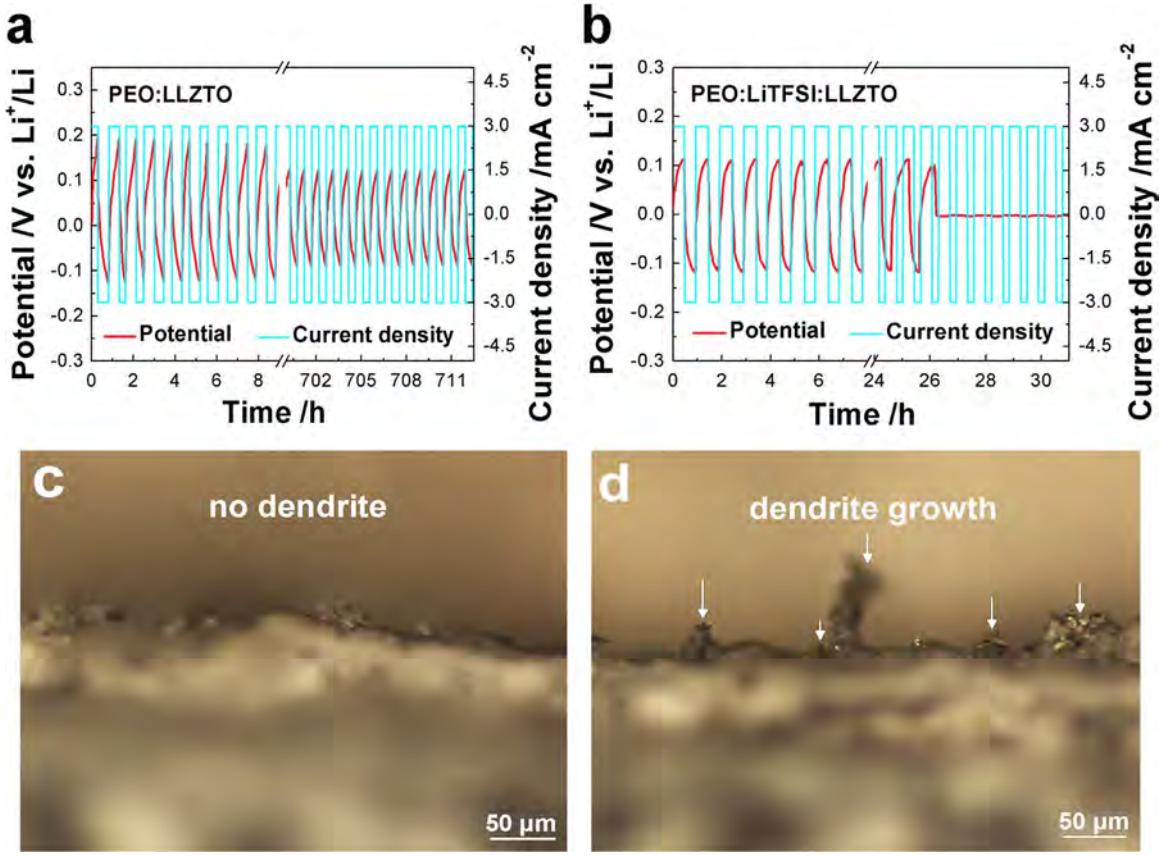

Fig. 4. Dendrite growth in the Li/PEO:LLZTO/Li and Li/PEO: LiTFSI:LLZTO/Li symmetrical cells. Galvanostatic cycles with a constant current density of 3.0 mA cm^{-2} for (a) Li/PEO:LLZTO/Li and (b) Li/PEO:LiTFSI:LLZTO/Li at 60 °C. Optical microscopy cross-sectional images of (c) Li/PEO:LLZTO/Li after cycling over 700 h (no dendrites) and (d) Li/PEO:LiTFSI:LLZTO/Li after cycling for about 25 h (large dendrites). The LLZTO particles used here are in size of D_{50}=43 nm.

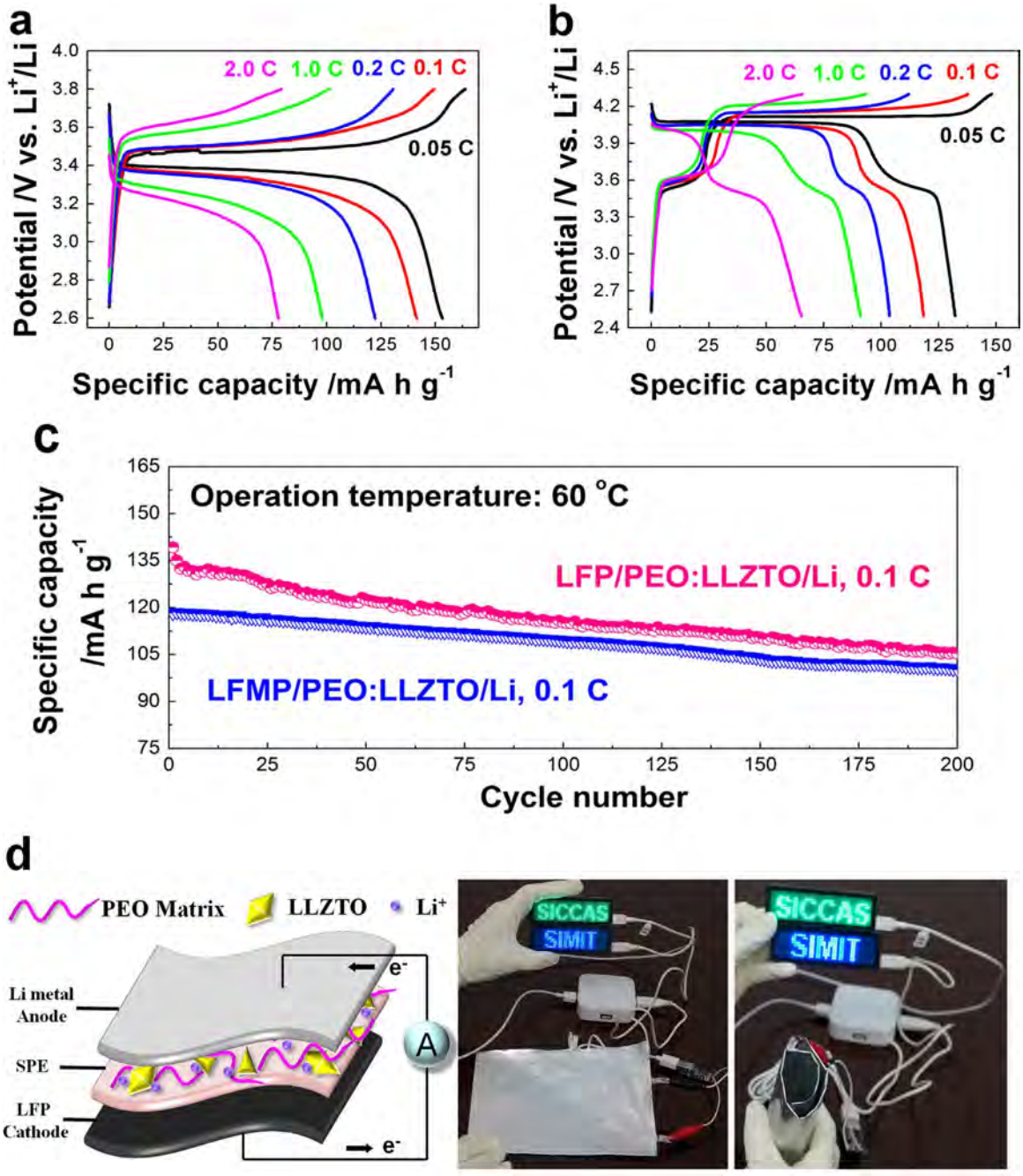

Fig. 5. Rate capability and cycle performance of the cells with the PEO: LLZTO membrane electrolyte. Galvanostatic charge-discharge curves at 0.05 C, 0.1 C, 0.2 C, 1.0 C, and 2.0 C for (a) LFP-based and (b) LFMP-based cells at 60 °C. (c) Cycle performance at 0.1 C for the LFP and LFMP-based cells at 60 °C. (d) Schematic image of the flexible pouch cell (LFP/PEO:LLZTO/Li) and illustration of the cell for powering the LEDs with the signals of "SIMIT" and "SICCAS".

short time. For the Li/PEO:LLZTO/Li cell, since LLZTO nanoparticles are well dispersed in the polymer matrix, the local current density at the electrolyte/anode interface is significantly reduced [47,48]. In addition, the Li-salt-free polymer does not allow the transport of Li^+ carriers, therefore, the accumulation of lithium in the insulating polymer is hampered and the continuous growth of lithium dendrites is suppressed at the electrolyte/anode interfaces. Due to the suppression of lithium dendrites, the cycle time for the Li/PEO:LLZTO/Li cell can be remarkably extended.

3.4. Cell performance of PEO:LLZTO membrane electrolyte

By combining the LFP and LFMP-based cathodes [49], SSLBs using the PEO:LLZTO membrane electrolytes in pouch cells of 0.1 Ah are fabricated. The galvanostatic charge and discharge cycles are assessed at 60 °C. As shown in Fig. 5a, the typical potential plateaus of 3.37 V and 3.52 V corresponding to discharge and charge of LFP at 0.05 C, respectively, can be clearly identified. The specific discharge capacity at 0.05 C is 153.3 mA h g^{-1}, which is 90% of the theoretical value. When the current densities are increased to 0.1 C, 0.2 C, 1.0 C, and 2.0 C, the specific discharge capacities diminish to 141.5 mA h g^{-1}, 122.3 mA h g^{-1}, 98.0 mA h g^{-1}, and 77.8 mA h g^{-1}, respectively. For the LFMP-based cells, the typical charge potentials are 3.65 V and 4.2 V and typical discharge potentials are 3.9 V and 3.5 V at 0.05 C as shown in Fig. 5b. The specific discharge capacity at 0.05 C is 132.1 mA h g^{-1}, which is 89% of the theoretical value. And as the current density increases, the specific discharge capacities

decrease to 118.2 mA h g^{-1}, 103.5 mA h g^{-1}, 91.1 mA h g^{-1}, and 65.3 mA h g^{-1} corresponding to 0.1 C, 0.2 C, 1.0 C, and 2.0 C, respectively. The cycle performance of the cells at 60 °C is also evaluated at the current density of 0.1 C (0.162 mA cm^{-2} for LFP-based cells and 0.156 mA cm^{-2} for LFMP-based cells) and shown in Fig. 5c. Both cells can be operated for more than 200 cycles with the capacity retention of 90% (1.46 mAh cm^{-2} for LFP-based cells and 1.41 mAh cm^{-2} for LFMP-based cells). Taking into account the weight and volume of the cells in scale of 0.1 Ah, the LFP-based cells offer energy densities of 345 Wh kg^{-1} (662 Wh L^{-1}, excluding the package weight or volume) and 133 Wh kg^{-1} (403 Wh L^{-1}, including the package weight or volume) whereas the LFMP-based cells provide energy densities of 405 Wh kg^{-1} (700 Wh L^{-1}, excluding the package weight or volume) and 159 Wh kg^{-1} (448 Wh L^{-1}, including the package weight or volume). Since the PEO:LLZTO membrane electrolytes are solid and flexible, the batteries based on them can be flexible and bendable as well, as shown in Fig. 5d. Even after folding into a cylindrical shape, the membrane-electrolyte-based battery can still power light-emitting diodes (LEDs) without noticeable dimming.

In the battery comprising the PEO:LLZTO membrane electrolyte, the nanoparticles with high ionic conductivity provide the percolated interfaces to increase the overall conductivity. The insulating PEO not only offers a flexible support but also suppresses growth of lithium dendrites. Although the addition of LLZTO nanoparticles improves the stability of polymer like PEO:LiTFSI from 4.25 V to over 4.7 V, the inevitable decomposition of the polymer may result in degraded stability of the PEO:LLZTO membrane with time. If a polymer with improved stability is available, the SSLBs can be constructed with enlarged voltage cathodes such as $LiNi_{0.5}Mn_{1.5}O_4$ to further increase the energy density.

4. Conclusions

Membrane electrolytes composed of Li-salt-free PEO and LLZTO nanoparticles in size of D_{50}=43 nm show the ionic conductivities of 2.1×10^{-4} S cm^{-1} at 30 °C and 5.6×10^{-4} S cm^{-1} at 60 °C. The improved conductivity is attributed to the interfacial effect at the polymer/LLZTO boundaries arising from percolation. The electrochemical window of greater than 4.7 V, Li^+ transference number of 0.46, and suppressed lithium dendrite growth indicate that the membranes are suitable for SSLBs. The cells consisting of the LFP as well as LFMP-based cathodes show good rate capability and cycle performance with high energy densities of 345 Wh kg^{-1} (662 Wh L^{-1}) and 405 Wh kg^{-1} (700 Wh L^{-1}) in pouch cells of 0.1 Ah excluding the package weight or volume, respectively. By using better polymers in conjunction with oxide electrolytes, the SSLBs have great potential to satisfy the high energy density and safety requirement for next-generation lithium batteries.

Acknowledgments

The authors would thank the financial supports from National Key Basic Research Program of China (Grant no. 2014CB921004), National Natural Science Foundation of China (Grant no. 51532002 & 61274136), Creative Research Groups of National Natural Science Foundation of China (No. 61321492), Program of Shanghai Academic/Technology Research Leader (16XD1404200), and City University of Hong Kong Applied Research Grant (ARG) Nos. 9667104 and 9667122.

Appendix A. Supplementary material

Supplementary data associated with this article can be found in the online version at http://dx.doi.org/10.1016/j.nanoen.2016.09.002.

References

[1] J.M. Tarascon, M. Armand, Nature 414 (2001) 359–367.
[2] N. Ohta, K. Takada, L. Zhang, R. Ma, M. Osada, T. Sasaki, Adv. Mater. 18 (2006) 2226–2229.
[3] M. Armand, J.M. Tarascon, Nature 451 (2008) 652–657.
[4] P. Hovington, M. Lagacé, A. Guerfi, P. Bouchard, A. Mauger, C.M. Julien, M. Armand, K. Zaghib, Nano Lett. 15 (2015) 2671–2678.
[5] S. Choudhury, R. Mangal, A. Agrawal, L.A. Archer, Nat. Commun. 6 (2015) 10101.
[6] D.O. Shin, K. Oh, K.M. Kim, K.Y. Park, B. Lee, Y.G. Lee, K. Kang, Sci. Rep. 5 (2015) 18053.
[7] M. Kotobuki, H. Munakata, K. Kanamura, Y. Sato, T. Yoshida, J. Electrochem. Soc. 157 (2010) A1076–A1079.
[8] Y. Tao, S. Chen, D. Liu, G. Peng, X. Yao, X. Xu, J. Electrochem. Soc. 163 (2016) A96–A101.
[9] J. Zhang, J. Zhao, L. Yue, Q. Wang, J. Chai, Z. Liu, X. Zhou, H. Li, Y. Guo, G. Cui, L. Chen, Adv. Energy Mater. 5 (2015) 1501082.
[10] N. Kamaya, K. Homma, Y. Yamakawa, M. Hirayama, R. Kanno, M. Yonemura, T. Kamiyama, Y. Kato, S. Kawamoto, A. Mitsui, Nat. Mater. 10 (2011) 682–686.
[11] Y. Kato, S. Hori, T. Saito, K. Suzuki, M. Hirayama, A. Mitsui, M. Yonemura, H. Iba, R. Kanno, Nat. Energy 1 (2016) 16030.
[12] Y. Deng, C. Eamea, J.N. Chotard, F. Lalère, V. Seznec, S. Emge, O. Pecher, C. P. Grey, C. Masquelier, M.S. Islam, J. Am. Chem. Soc. 137 (2015) 9136–9145.
[13] Z. Deng, B. Radhakrishnan, S.P. Ong, Chem. Mater. 27 (2015) 3749–3755.
[14] G.-y Adachi, N. Imanaka, H. Aono, Adv. Mater. 8 (1996) 127–135.
[15] P. Knauth, Solid State Ion. 180 (2009) 911–916.
[16] J.B. Goodenough, P. Singh, J. Electrochem. Soc. 162 (2015) A2387–A2392.
[17] E. Quartarone, P. Mustarelli, A. Magistris, Solid State Ion. 110 (1998) 1–14.
[18] J.H. Ahn, G.X. Wang, H.K. Liu, S.X. Dou, J. Power Sources 119–121 (2003) 422–426.
[19] F. Deng, X. Wang, D. He, J. Hu, C. Gong, Y.S. Ye, X. Xie, Z. Xue, J. Mem. Sci. 491 (2015) 82–89.
[20] F. Han, Y. Zhu, X. He, Y. Mo, C. Wang, Adv. Energy Mater. 6 (2016) 1501590.
[21] K. Takada, Acta Mater. 61 (2013) 759–770.
[22] A. Manthiram, L. Li, Adv. Energy Mater. 5 (2015) 1401302.
[23] L. Cheng, C.H. Wu, A. Jarry, W. Chen, Y. Ye, J. Zhu, R. Kostecki, K. Persson, J. Guo, M. Salmeron, G. Chen, M. Doeff, ACS Appl. Mater. Interfaces 7 (2015) 17649–17655.
[24] A. Sharafi, H.M. Meyer, J. Nanda, J. Wolfenstine, J. Sakamoto, J. Power Sources 302 (2016) 135–139.
[25] J.E. Ni, E.D. Case, J.S. Sakamoto, E. Rangasamy, J.B. Wolfenstine, J. Mater. Sci. 47 (2012) 7978–7985.
[26] S. Yu, R.D. Schmidt, R. Garcia-Mendez, E. Herbert, N.J. Dudney, J. B. Wolfenstine, J. Sakamoto, D.J. Siegel, Chem. Mater. 28 (2016) 197–206.
[27] Y. Li, Z. Wang, C. Li, Y. Cao, X. Guo, J. Power Sources 248 (2014) 642–646.
[28] F. Du, N. Zhao, Y. Li, C. Chen, Z. Liu, X. Guo, J. Power Sources 300 (2015) 24–28.
[29] R.P. eschiglian, G. Torsi, Chromatographia 40 (1995) 467–473.
[30] C.W. Nan, Prog. Mater. Sci. 37 (1993) 1–116.
[31] A.J. Bhattacharyya, J. Maier, Adv. Mater. 16 (2004) 811–814.
[32] H. Yamada, A.J. Bhattacharyya, J. Maier, Adv. Func. Mater. 16 (2006) 525–530.
[33] C.W. Nan, Y. Shen, J. Ma, Annu. Rev. Mater. Sci. 40 (2010) 131–151.
[34] B. Kumar, L.G. Scanlon, J. Power Sources 52 (1994) 261–268.
[35] D.F. Shriver, P.G. Bruce, Chemistry of Solid State Materials, in: B. Dunn, J.W. Goodby (Eds.), Cambridge University Press, UK, 1997, pp. 96–97.
[36] K.M. Abraham, Z. Jiang, B. Carroll, Chem. Mater. 9 (1997) 1978–1988.
[37] J.W. Fergus, J. Power Sources 195 (2010) 4554–4569.
[38] W. Liu, N. Liu, J. Sun, P.C. Hsu, Y. Li, H.W. Lee, Y. Cui, Nano Lett. 15 (2015) 2740–2745.
[39] D. Lin, Y. Liu, Z. Liang, H.W. Lee, J. Sun, H. Wang, K. Yan, J. Xie, Y. Cui, Nano Lett. 16 (2016) 459–465.
[40] F. Gray, M. Armand, in: C. Daniel, J.O. Besenhard (Eds.), Handbook of Battery Materials, Wiley-VCH Verlag GmbH & Co. KGaA, Germany, 2008, pp. 627–637.
[41] N. Salem, Y. Abu-Lebdeh, in: Y. Abu-Lebdeh, I. Davidson (Eds.), Nanotechnology for Lithium-ion Batteries, Springer, New York, 2013, pp. 223–226.
[42] J. Maier, Prog. Solid State Chem. 23 (1995) 171–263.
[43] A. Selvaggi, F. Croce, B. Scrosati, J. Power Sources 32 (1990) 389–396.
[44] F. Capuano, F. Croce, B. Scrosati, J. Electrochem. Soc. 138 (1991) 1918–1922.
[45] W. Wieczorek, A. Zalewska, D. Raducha, Z. Florjańczyk, J.R. Stevens, J. Phys. Chem. B 102 (1998) 352–360.
[46] Y. Ren, Y. Shen, Y. Lin, C.W. Nan, Electrochem. Commun. 57 (2015) 27–30.
[47] D. Lin, Y. Liu, Z. Liang, H.W. Lee, J. Sun, H. Wang, K. Yan, J. Xie, Y. Cui, Nat. Nanotechnol. 32 (2016).
[48] X. Cheng, T. Hou, R. Zhang, H. Peng, C. Zhao, J. Huang, Q. Zhang, Adv. Mater. 28 (2016) 2888–2895.
[49] M.S. Islam, A. Craig, J. Fisher, Chem. Soc. Rev. 43 (2014) 185.

Jingxian Zhang obtained her Ph.D. in 2014 from Chengdu Institute of Organic Chemistry, Chinese Academy of Sciences (CAS). Currently, she is a postdoctoral researcher at State Key Laboratory of Functional Materials for Informatics, Shanghai Institute of Microsystem and Information Technology, Chinese Academy of Sciences (CAS). Her research interest mainly focuses on the design and development of advanced materials for solid-state lithium batteries.

Ning Zhao received his Ph.D. in material physics and chemistry from Shanghai Institute of Ceramics, Chinese Academy of Sciences (CAS). Under the supervision of Prof. Xiangxin Guo, Ning Zhao has been actively involved in Li-O_2 battery researches, and the fundamental researches on Na-O_2 battery. His current research focuses on solid electrolytes and rechargeable all-solid-state battery.

Miao Zhang received her Ph.D. in microelectronics and solid-state electronics from Shanghai Institute of Microsystem and Information Technology, Chinese Academy of Sciences (CAS) in 1998. She is currently working as a professor of Shanghai Institute of Microsystem and Information Technology, Chinese Academy of Sciences (CAS). Her research interests focus on high mobility semiconductors, silicon-on-insulator materials, semiconductors for energy storage applications, etc.

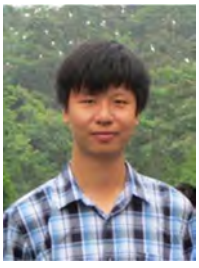

Yiqiu Li received his Ph.D. in Material Science and Engineering in 2011 from Wuhan University of Technology. From 2012 to 2014, he worked as a postdoctor in Shanghai Institute of Ceramics, Chinese Academy of Sciences (CAS). He is now a research assistant in Shanghai Institute of Ceramics, Chinese Academy of Sciences (CAS). His research interests include solid electrolytes, electrodes and solid-solid interfaces for all-solid-state lithium-ion batteries.

Paul K. Chu received his Ph.D. in chemistry from Cornell University and is Chair Professor of Materials Engineering in the Department of Physics and Materials Science at City University of Hong Kong. He is Fellow of the American Physical Society (APS), American Vacuum Society (AVS), Institute of Electrical and Electronics Engineers (IEEE), Materials Research Society (MRS), and Hong Kong Institution of Engineers (HKIE). He is also Fellow of the Hong Kong Academy of Engineering Sciences (HKAES). His research interests are quite diverse encompassing plasma surface engineering, materials science and engineering, surface science, and functional materials.

Xiangxin Guo received his Ph.D. from Institute of Physics, Chinese Academy of Sciences (CAS) in 2000. As a postdoctoral scientist, he continued research at the Max Planck Institute for Solid State Research, at the Paul Drude Institute for Solid State Electronics, and at the European Synchrotron Radiation Facility. He then worked as a staff scientist at the Max Planck Institute for Solid State Research, before joining the Shanghai Institute of Ceramics, where he is currently a full professor and a leader of a research group. His research focuses on metal-air batteries, solid-state lithium batteries, and heterostructure-based solid-state ionic devices.

Zengfeng Di received his Ph.D. in microelectronics and solid-state electronics from Shanghai Institute of Microsystem and Information Technology, Chinese Academy of Sciences (CAS) in 2006. He is now working as a professor of Shanghai Institute of Microsystem and Information Technology, Chinese Academy of Sciences (CAS). His research interests focus on ion beam technology, high mobility semiconductors including two dimensional materials, silicon-on-insulator materials, and energy materials.

Xi Wang received his Ph.D. in materials and physics from Shanghai Institute of Microsystem and Information Technology, Chinese Academy of Sciences (CAS) in 1993. He is currently a professor and a director of Shanghai Institute of Microsystem and Information Technology, Chinese Academy of Sciences (CAS). His research interests focus on ion beam technology, silicon-on-insulator wafer manufacturing, various applications of silicon-on-insulator materials, and semiconductor materials for energy application.

Hong Li obtained his Ph.D. from Institute of Physics, Chinese Academy of Sciences (CAS) in 1999. Currently, he is a professor in Institute of Physics, Chinese Academy of Sciences (CAS). His research interest includes fundamental researches in batteries, such as transport of ions and electrons, size effect, interface phenomena, structure evolution as well as application researches including Si-based anode for high energy density Li-ion batteries, solid lithium batteries and their failure analysis.

Supporting Information

Flexible and Ion-Conducting Membrane Electrolytes for Solid-State Lithium Batteries: Dispersion of Garnet Nanoparticles in Insulating Polyethylene Oxide

Jingxian Zhang [a,b], Ning Zhao [b], Miao Zhang [a], Yiqiu Li [b], Paul K. Chu [c], Xiangxin Guo [b,*], Zengfeng Di [a,*], Xi Wang [a], and Hong Li [d]

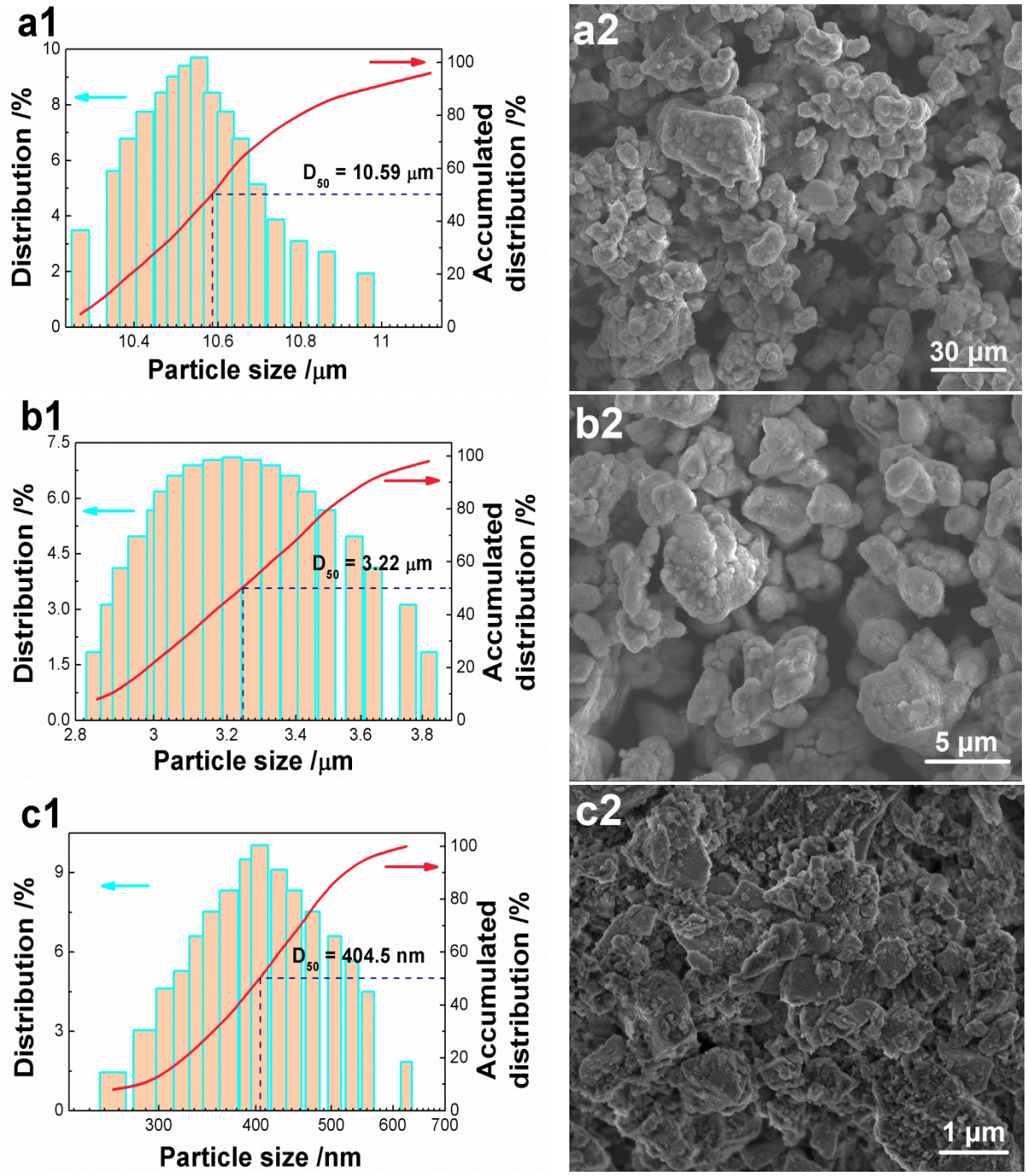
a1
Distribution /%
Accumulated distribution /%
D50 = 10.59 μm
Particle size /μm
a2
30 μm
b1
Distribution /%
Accumulated distribution /%
D50 = 3.22 μm
Particle size /μm
b2
5 μm
c1
Distribution /%
Accumulated distribution /%
D50 = 404.5 nm
Particle size /nm
c2
1 μm

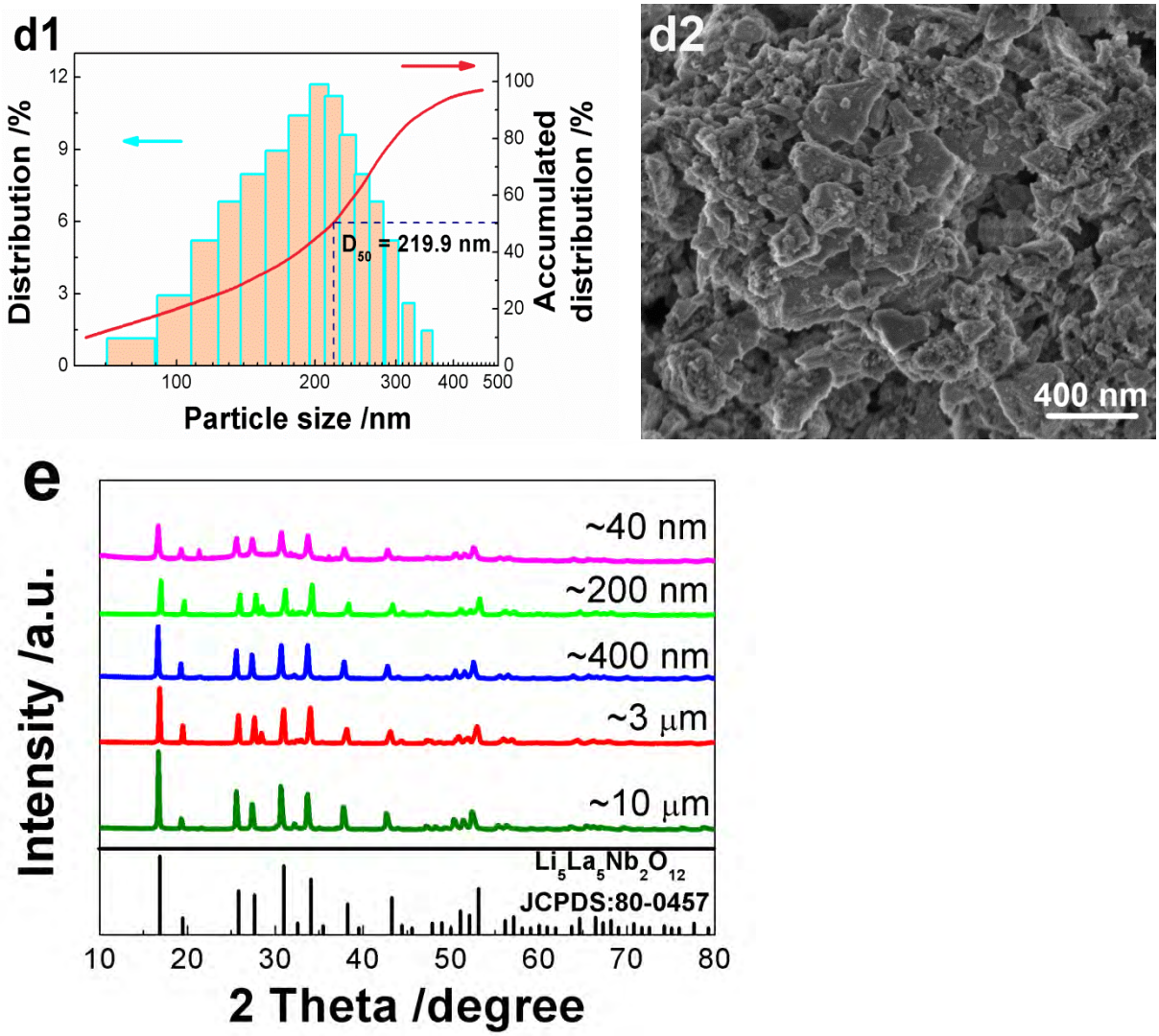

Fig. S1. (a)-(d) Size distributions and SEM images of the LLZTO particles obtained by ball-milling processes. (e) XRD spectra of LLZTO particles with different sizes.

From size distributions and SEM images of LLZTO particles with different sizes shown in Fig. S1, it can be deduced that the diameters of LLZTO particles in terms of D_{50} are 10.59 μm, 3.22 μm, 404.5 nm and 219.9 nm, respectively.

The diffraction patterns of the LLZTO particles with five different sizes show that they have a typical cubic garnet phase similar to $Li_5La_5Nb_2O_{12}$ (JCPDS 80-0457) [1] and no obvious impurity phases are found.

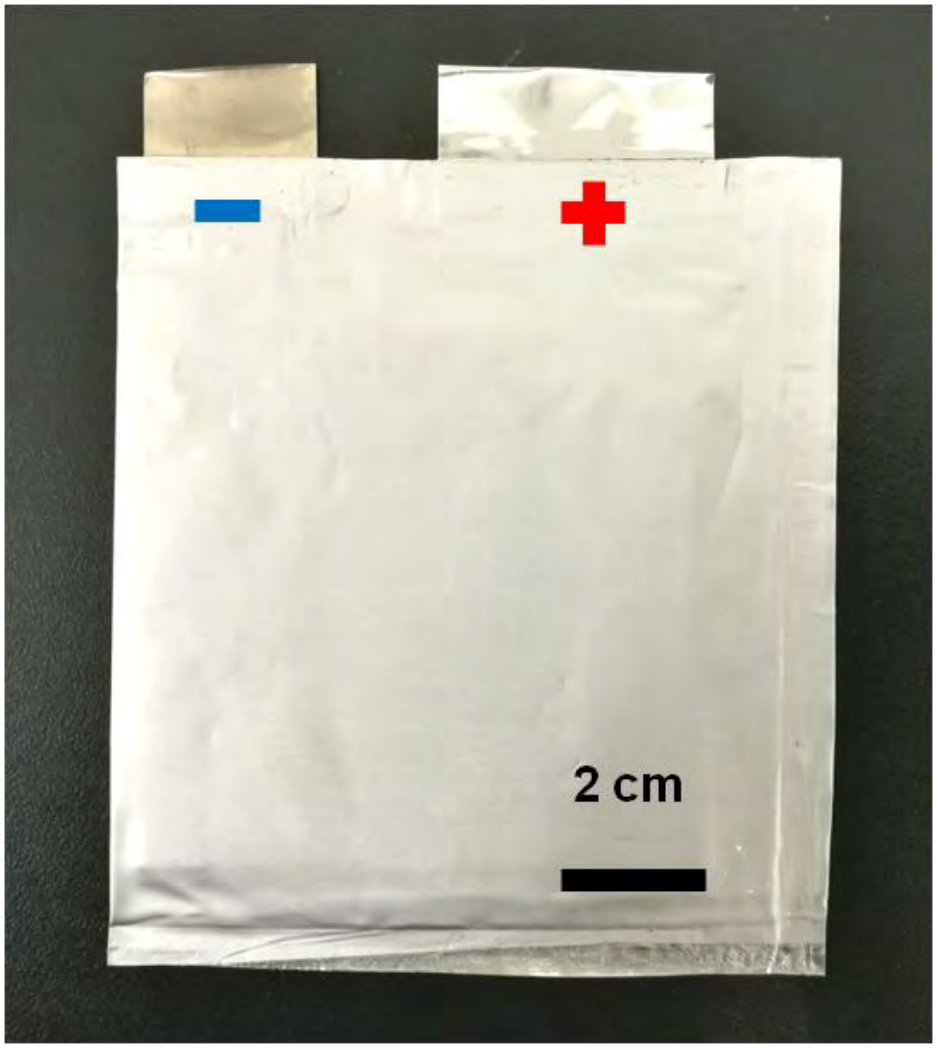

Fig. S2. Photo of a typical pouch cell with the capacity of 0.1 Ah.

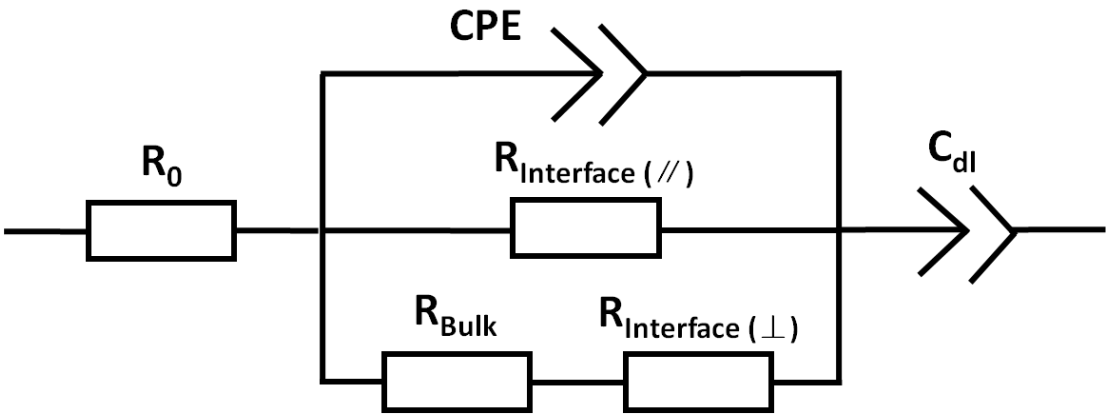

Fig. S3. Equivalent circuit for the PEO:LLZTO membrane electrolyte.

The equivalent circuit for the PEO:LLZTO membrane electrolyte is illustrated in Fig. S3. $R_{Interface}$ is composed of $R_{Interface(//)}$ and $R_{Interface(\perp)}$, which correspond to the resistances parallel and perpendicular to the interface between PEO and LLZTO, respectively. And, R_0 and R_{Bulk} correspond to the resistances of the contacts and the electrolyte bulk, respectively. In addition, CPE is denoted as constant phase element, and C_{dl} represents double layer capacitor between electrode and electrolyte at the low frequencies.

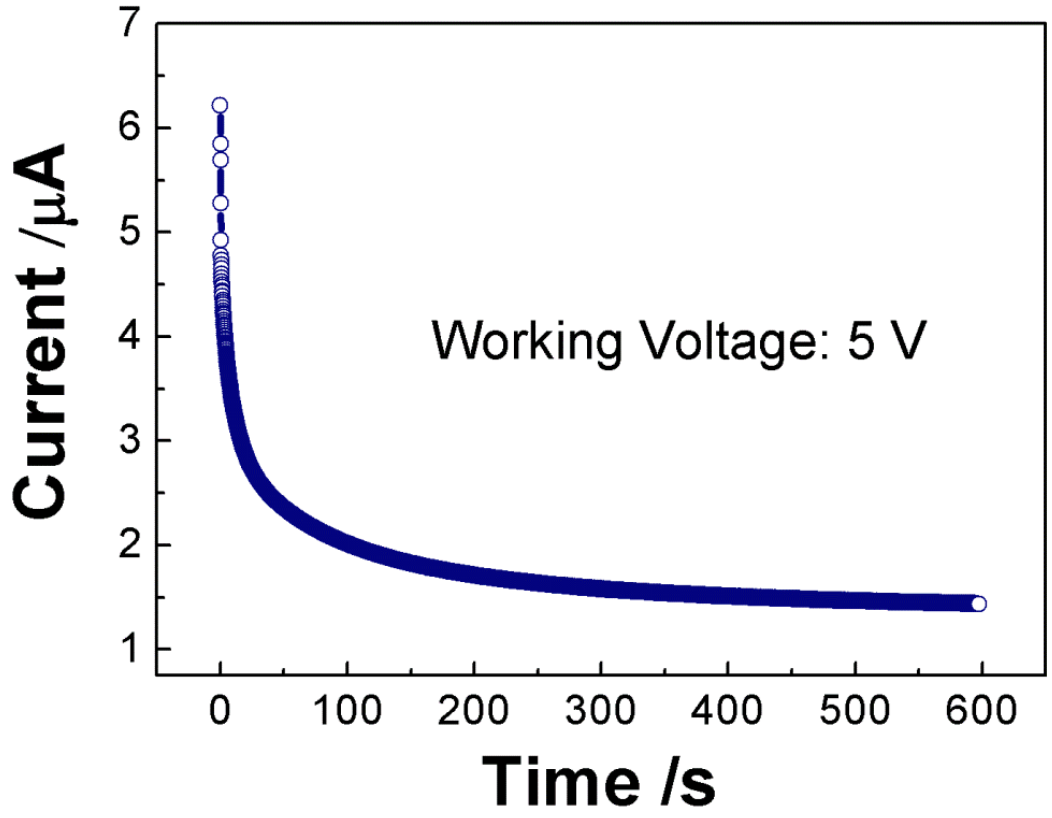

Fig. S4. Potentiostatic polarization current as a function of time at room temperature of the PEO:LLZTO membrane electrolyte.

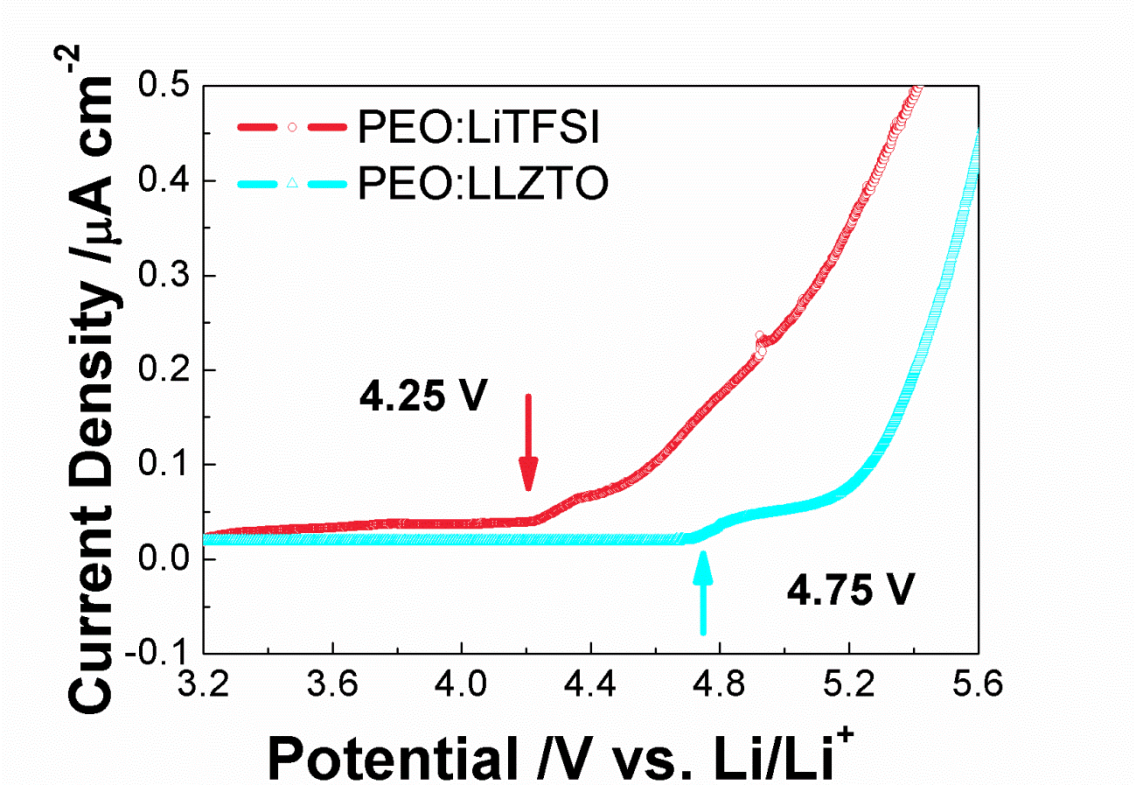

Fig. S5. LSV scans at a scanning rate of 10 mV s^{-1} for PEO:LiTFSI and PEO:LLZTO membrane with 12.7 vol% LLZTO (partial enlargement of Fig. 3a). It is clearly shown that the oxidation voltages of PEO:LiTFSI and PEO:LLZTO start at 4.25 V and 4.75 V, respectively.

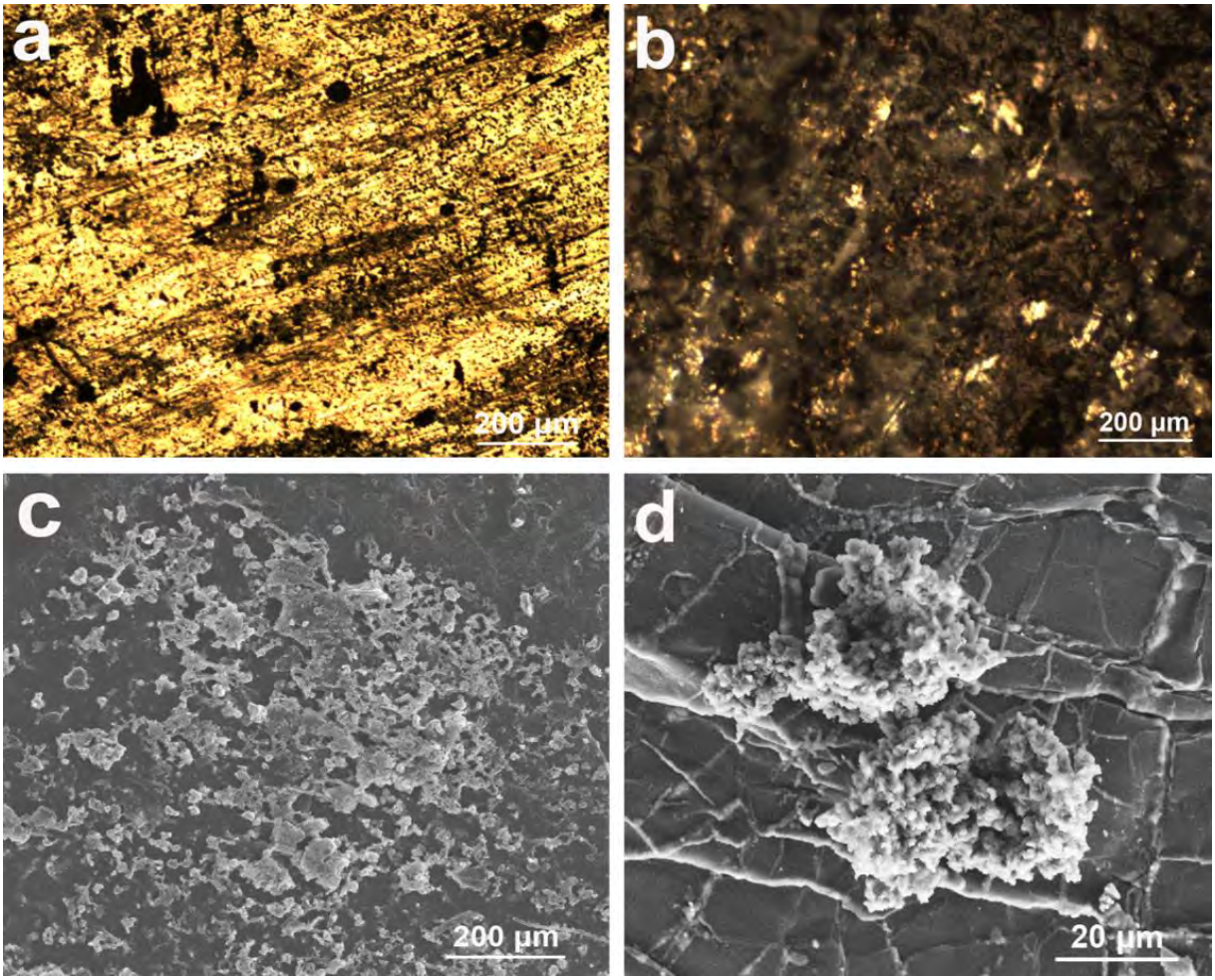

Fig. S6. Dendrite growth in the Li/PEO:LLZTO/Li and Li/PEO:LiTFSI:LLZTO/Li symmetrical cells. Optical microscopy plane view images for Li metal of (a) Li/PEO:LLZTO/Li cell after cycling at a current density of 3 mA cm^{-2} over 700 h and (b) Li/PEO:LiTFSI:LLZTO/Li cell after cycling at a current density of 3 mA cm^{-2} for about 25 h. (c) and (d) are the SEM images of the dendrites in the Li/PEO:LiTFSI:LLZTO/Li cell at different resolution.

Calculation of lithium-ion transference number

The lithium transference number (T_{Li^+}) are calculated according to $T_{Li^+} = \frac{I_{(t=\infty)}(\Delta V - I_{(t=0)}R_{(t=0)})}{I_{(t=0)}(\Delta V - I_{(t=\infty)}R_{(t=\infty)})}$, where ΔV is the applied DC polarization voltage (10 mV), $I_{(t=0)}$ and $I_{(t=\infty)}$ are the initial and steady currents during polarization, $R_{(t=0)}$ and $R_{(t=\infty)}$ are the resistance values of the PEO:LLZTO electrolyte before and after polarization measured by the impedance spectroscopy [2,3]. The results are listed in the following.

Table S1. Calculated T_{Li^+} for PEO:LLZTO membrane samples with different volume fractions of the LLZTO.

Sample	$I_{(t=0)}/\mu A$	$I_{(t=\infty)}/\mu A$	$R_{(t=0)}/\Omega$	$R_{(t=\infty)}/\Omega$	T_{Li^+}
PEO:LiTFSI	34.3	9	62.4	62.1	0.22
PEO:LLZTO-5.2	7.1	2.2	51.9	52	0.31
PEO:LLZTO-8.6	3	1.1	37.2	37.5	0.37
PEO:LLZTO-10.5	5.7	2.4	30.8	30.5	0.42
PEO:LLZTO-12.7	6.1	2.8	17.7	17.9	0.46
PEO:LLZTO-15.1	7.2	3.1	22.9	22.3	0.43
PEO:LLZTO-17.9	4.6	1.8	29.5	29.1	0.39
PEO:LLZTO-21.1	8.1	2.7	34.6	34.8	0.33

References

[1] J. L. Allen, J. Wolfenstine, E. Rangasamy, J. Sakamoto, J. Power Sources 206 (2012) 315-319.

[2] F. Capuano, F. Croce, B. Scrosati, J. Electrochem. Soc. 138 (1991) 1918-1922.

[3] H. Zhang, C. Liu, L. Zheng, F. Xu, W. Feng, H. Lim, X. Huang, M. Armand, J. Nie, Z. Zhou, Electrochim. Acta 133 (2014) 529-538.